

## Inner Bremsstrahlung from $A^{37}$ \*

TORSTEN LINDQVIST† AND CHIEN-SHUNG WU  
Columbia University, New York, New York

(Received December 20, 1954)

The continuous gamma-ray spectrum (inner bremsstrahlung), accompanying orbital electron capture in  $A^{37}$ , has been reinvestigated by the method of scintillation spectroscopy with particular emphasis on the low energy region. The absorption between the source and the NaI crystal is only due to two one-mil Al foils. After correcting for NaI crystal detection efficiency, the geometrical factor, the ratio of photoelectric cross section to total cross section, Compton electron backscattering, iodine x-ray escape, absorption and resolution, it is found that the intensity of the extremely low-energy photons is much greater than can be accounted for by Morrison and Schiff's treatment. A better agreement can be obtained if one considers the  $p$ -electron capture, and takes the Coulomb effect into consideration as shown by Glauber and Martin.

### INTRODUCTION

THE continuous gamma-ray spectrum (inner bremsstrahlung) accompanying orbital electron capture was first investigated theoretically by Morrison and Schiff.<sup>1</sup> Later Jauch<sup>2</sup> extended the theoretical investigation with minor revisions. However, both studies take account only of the  $K$ -electron capture. Recent investigations<sup>3-5</sup> on the distribution of inner bremsstrahlung from electron capture processes in  $Fe^{55}$ ,  $Cs^{131}$ , and  $Ge^{71}$  all have shown that the aforementioned calculations are not adequate in interpreting the low-energy region of the distribution. The observed distributions show a large increase in intensity at low energies instead of dropping to zero intensity as called for by Morrison and Schiff's predictions. The region where the deviation from Morrison and Schiff's prediction becomes noticeable is different for different elements.

Earlier experiments<sup>6,7</sup> on the inner bremsstrahlung from  $A^{37}$  have concentrated their efforts on the determination of the maximum available energy but very little attention has been paid to its distribution in the low-energy region. Therefore it was highly desirable to reinvestigate this nuclide with emphasis on the shape of the spectrum particularly in the low-energy region.

$A^{37}$  decays to  $Cl^{37}$  by pure electron-capture with a half-life of 34 days. There are no  $\beta^-$  or  $\beta^+$  and no  $\gamma$  rays. According to the shell model it is a  $d_{3/2} \rightarrow d_{3/2}$  transition, i.e., an allowed transition. The decay energy has been calculated from the threshold energy<sup>8</sup> of the  $Cl^{37}(p,n)A^{37}$  reaction to be  $816 \pm 4$  kev which is in good agreement

with the value  $815 \pm 20$  kev determined from the maximum energy of the inner bremsstrahlung.<sup>5,6</sup> The ratio of the total number of bremsstrahlung photons to the total number of  $K$ -captures is given for  $1S$  capture by

$$\int_0^{k_0} \frac{N(k)dk}{N_e} = \frac{\alpha}{12\pi} \left( \frac{W_0}{m_0c^2} \right)^2,$$

where  $W_0$  is the maximum disintegration energy. It is proportional to  $W_0^2$ , and therefore the intensity of the  $A^{37}$  inner bremsstrahlung is expected to be relatively high.

### I. GLAUBER-MARTIN THEORY<sup>9</sup>

This theory takes into consideration (1) both magnetic and electric radiation, (2) both  $S$ - and  $P$ -electron capture, (3) all effects of the Coulomb field. It is shown that the electric dipole radiation accompanying the capture of  $p$ -electrons is primarily responsible for the large intensity increase at low energies. The electric dipole radiation is relatively more important for larger nuclear charge. In Table I are listed the isotopes whose inner bremsstrahlung has been investigated experi-

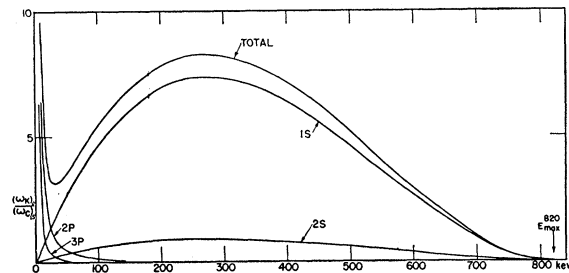


FIG. 1. The distribution of the bremsstrahlung radiations from  $1S$ -,  $2S$ -,  $2P$ -, and  $3P$ -electron capture in  $A^{37}$  according to the Glauber-Martin theory.

$$\frac{(\omega_k)dk}{(\omega_c)_{1S}} = \frac{\alpha}{\pi} \left( \frac{Z^2\alpha^2}{2} \right)^2 \left[ 1 - \frac{x - (E_l - E_{1S})}{x_{\max}} \right]^2 I_l(x) dx,$$

where  $x$  is in  $(Z^2 \cdot Ry)$  units;  $x_{\max}$  is the upper limit of the photon energy; and  $I_l(x)$  is a theoretical function tabulated in P. C. Martin's thesis.

<sup>9</sup> R. J. Glauber and P. C. Martin, Phys. Rev. **95**, 572 (1954).

\* This work was supported by the U. S. Atomic Energy Commission.

† Now at Physics Department, University of Uppsala, Sweden.

<sup>1</sup> P. Morrison and L. I. Schiff, Phys. Rev. **58**, 24 (1940).

<sup>2</sup> J. M. Jauch, Oak Ridge National Laboratory ORNL-1102, 1951 (unpublished).

<sup>3</sup> L. Madansky and F. Rasetti, Phys. Rev. **94**, 407 (1954).

<sup>4</sup> B. Saraf, Phys. Rev. **94**, 642 (1954).

<sup>5</sup> B. Saraf, Phys. Rev. **95**, 97 (1954).

<sup>6</sup> Anderson, Wheeler, and Watson, Phys. Rev. **90**, 606 (1953).

<sup>7</sup> Emmerich, Singer, and Kurbatov, Phys. Rev. **94**, 113 (1954).

<sup>8</sup> Richards, Smith, and Browne, Phys. Rev. **80**, 524 (1950); Schoenfeld, Duborg, Preston, and Goodman, Phys. Rev. **85**, 873 (1952).

TABLE I. Some pertinent information on the inner bremsstrahlung from the electron capture process in  $\text{Fe}^{55}$ ,  $\text{Cs}^{131}$ ,  $\text{Ge}^{71}$ , and  $\text{A}^{37}$ .

Isotope	$E_{\text{max}}$ kev	$E_K$ kev	$E_i$ kev	Reference
$\text{Fe}^{55}$	220	5.9	60	3
$\text{Cs}^{131}$	350	33	100-150	4
$\text{Ge}^{71}$	230	10	40-60	5
$\text{A}^{37}$	820	2.8	30	Fig. 7

mentally.  $E_i$  denotes the region below which there is a deviation from Morrison and Schiff's prediction.  $E_K$  is the  $K$ -ionization potential.

In Fig. 1 is shown the distribution of the radiations from  $1S$ -,  $2S$ -,  $2P$ -, and  $3P$ -electron capture according to the Glauber-Martin theory. The general expression for the radiative  $l$ -events  $(\omega_k)_l$  per  $1S$ -electron capture  $(\omega_c)_{1S}$  is

$$\frac{(\omega_k)_l dk}{(\omega_c)_{1S}} = \frac{\alpha (Z^2 \alpha^2)^2}{\pi (2)} \left[ 1 - \frac{x - (E_l - E_{1S})}{x_{\text{max}}} \right]^2 I_l(x) dx \quad (1)$$

or

$$\frac{(\omega_k)_l dk}{(\omega_c)_{1S}} = \frac{\alpha Z^2 \alpha^2}{\pi 2m} \left[ 1 - \frac{x - (E_l - E_{1S})}{x_{\text{max}}} \right]^2 I_l \left( \frac{k}{\frac{1}{2} Z^2 \alpha^2 m} \right) dk, \quad (1')$$

where  $x$  is the photon energy given in units of  $Z^2 R y = Z^2 \times 13.5 \text{ eV}$ ;  $I_l(x)$  is a theoretical function tabulated in Martin's thesis<sup>10</sup>;  $x_{\text{max}}$  is the upper limit of the photon energy. In the case of radiation from  $1S$ -capture, Eq. (1) reduces to the old Morrison-Schiff theory:

$$\begin{aligned} \frac{(\omega_k)_{1S} dk}{(\omega_c)_{1S}} &= \frac{\alpha}{\pi} \left[ 1 - \frac{x}{x_{\text{max}}} \right]^2 \frac{k}{m} d \left( \frac{k}{m} \right) \\ &= \frac{\alpha}{\pi} \left( \frac{W}{m} \right)^2 \left[ 1 - \frac{k}{W} \right]^2 \frac{k}{W} d \frac{k}{W}. \quad (2) \end{aligned}$$

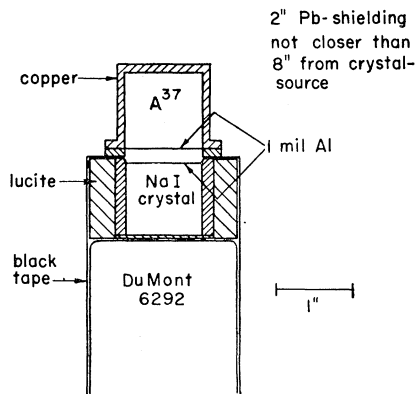


FIG. 2. Experimental arrangement.

<sup>10</sup> P. C. Martin, thesis, Harvard University, May, 1954 (unpublished).

For the radiation from  $2S$ -capture, one only takes  $\frac{1}{3}$  of the  $1S$ -intensity. For the  $2P$ - and  $3P$ -captures, the function  $I_l(x)$  is more complicated. The results shown in Fig. 1 are taken from a table given in Martin's thesis.<sup>10</sup> Fig. 1 shows also the sum of all contributions for the case of  $\text{A}^{37}$ . The marked increase in intensity starts at about 30 kev.

## II. EXPERIMENTAL ARRANGEMENT

The experimental arrangement is shown in Fig. 2. The  $\text{A}^{37}$  gas is contained in a copper cylinder of diameter 1 in., height 1 in., with a 1-mil Al window. The NaI crystal, of diameter 1 in. and height 1 in., is permanently canned in an aluminum container with a MgO reflector

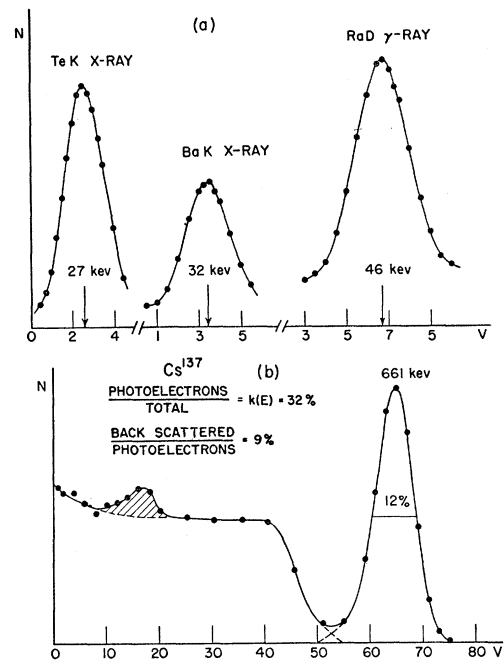


FIG. 3. (a) The low-energy calibrations. (b) An example of a complete gamma-ray spectrum used to determine the ratio of photo cross section to total cross section.

on its side wall. The top surface through which the radiation enters is covered with a 1-mil Al foil only. The total amount of absorbing material between source and crystal is 2 mils of Al. The gas container is placed as close to the crystal as possible. Since the source has a finite volume it was impossible to obtain all the correction curves with this geometry. As an approximation it was assumed that a point-source located in the center of an identical gas-container would represent the proper geometry. The crystal is mounted on a DuMont 6292 photomultiplier-tube. The arrangement gives a resolution of 12% at the gamma-ray energy 661 kev. The pulses are amplified in a nonblocking linear amplifier and the spectrum is analyzed with a pulse-height analyzer. The energy calibration is carried out by using

x-radiations of Te, Ba, and Hg and gamma-radiations of RaD, Hg<sup>203</sup>, Cr<sup>51</sup>, I<sup>126</sup>, Au<sup>198</sup>, Cu<sup>64</sup>, Na<sup>22</sup>, Cs<sup>137</sup>, etc. The linearity throughout the region used is good. Figure 3(a) shows some of the low-energy calibrations.

### III. SCINTILLATION TECHNIQUE APPLIED TO CONTINUOUS GAMMA-RAY SPECTRUM

In order to interpret the experimental data from a scintillation spectrometer measurement, it is necessary to study carefully the various effects in the crystal and from the surrounding material. These effects combine to affect the observed experimental spectrum. Therefore it is very difficult to analyze correctly in this manner. However, in the few cases where a theoretical prediction of its distribution exists, it is preferable to apply all the corrections due to the crystal effects to the theoretical distribution and compare it with the experimentally observed spectrum. The corrections applied to the theoretical distribution as shown in Fig. 4 are the following:

#### A. $\gamma$ -Detection Efficiency Including the Geometrical Factor

For source-crystal distances of the order of magnitude used in this experiment, namely  $\frac{1}{2}$  in., the geometrical factor becomes very important. For instance, when the efficiency for a normally incident beam on this particular crystal at 600 keV is 70%, it is only 40% for a source-crystal distance of  $\frac{1}{2}$  in. The  $\gamma$ -efficiency curve used is shown in Fig. 5(a), which is taken from Novey, since our geometrical arrangement is very similar to his. The resulting distribution after the efficiency correction is shown as curve A in Fig. 4.

#### B. Fractions of Photons Detected with Full Energy

Because of the presence of the Compton effect, all photons are not detected with their full energy. The ratio of photo cross section to total cross section is energy-dependent and should be determined for a number of energies throughout the region under identical conditions; for example, see Fig. 3(b). The region below 250 keV is not covered with experimental points, but fortunately the contribution from Compton electrons for energies below 250 keV is small. The curve obtained [Fig. 5(b)] can be checked together with the  $\gamma$ -efficiency curve by measuring the relative intensity of two  $\gamma$  rays where the intensity ratio is well known from other experiments. This was done by using the two  $\gamma$  rays of I<sup>126</sup> of 380 keV and 650 keV, their intensity ratio being determined as 1:1.<sup>11</sup> The agreement with this ratio was rather good. The distribution curve due to the contribution of these full-energy pulses is shown as curve B in Fig. 4.

<sup>11</sup> M. L. Perlman and Joan P. Welker, Phys. Rev. **95**, 133 (1954).

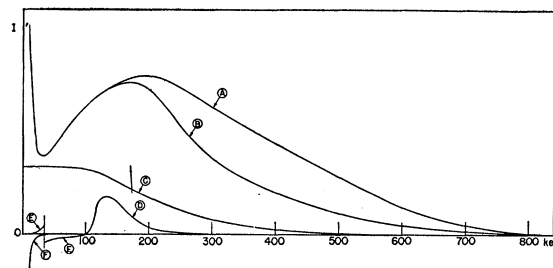


FIG. 4. Corrections to the theoretical distribution. NaI crystal; 1 in. diam.  $\times$  1 in. height; source-crystal  $\frac{1}{2}$  in. (a) Theoretical curve corrected for  $\gamma$  efficiency. (b) The distribution curve due to photoelectrons. (c) The Compton-electrons. (d) Backscattered photons. (e) Escape-effect. (f) Absorption.

#### C. Compton Electrons

The fraction of photons detected with energy less than their full energy can also be determined from Fig. 5(b). If the fraction of photons detected with full energy is  $p(E_\gamma)$ , it is obvious that the fraction of photons detected with less than full energy is  $[1 - p(E_\gamma)]$ . This correction becomes very important when there are photons of high energy present as in this case.

The number of photons of energy  $E_\gamma$  absorbed in the crystal is  $N_a(E_\gamma)$ . The number of Compton-electrons ranging from energy zero to  $E_\gamma^*$ , where  $E_\gamma^*$  is the maximum Compton-electron energy (the Compton peak), is  $N_a(E_\gamma)[1 - p(E_\gamma)]$ . The probability<sup>12</sup> that such a Compton-electron will have an energy between  $E$  and  $E + dE$  is a function  $C(E, E_\gamma)$ . The total number of Compton-electrons at energy  $E$  due to all incoming

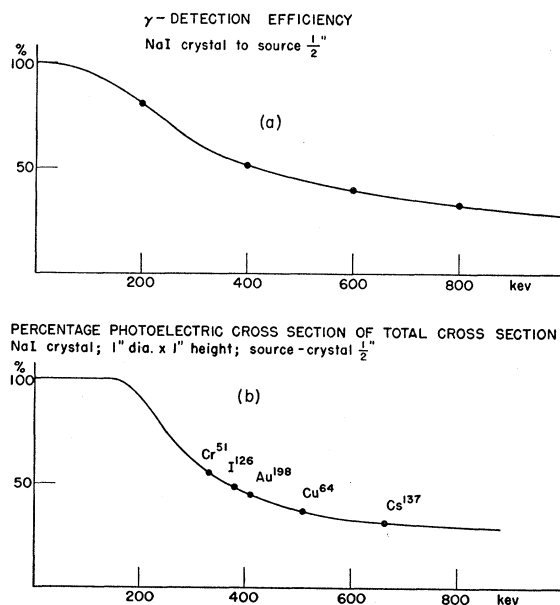


FIG. 5. (a)  $\gamma$ -detection efficiency. (b) The percentage of the photoelectric cross section of the total cross section vs energy.

<sup>12</sup> K. Lidén and N. Starfelt, Arkiv Fysik **7**, No. 36 (1954).

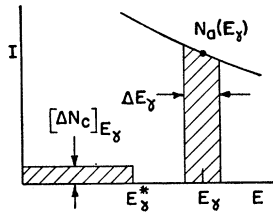


FIG. 6. Illustration of the method used for the calculation of the Compton contribution.

photons from energy zero to  $E_{\gamma, \max}$  is

$$N_c = \int_0^{E_{\max}} C(E, E_\gamma) N_a(E_\gamma) [1 - p(E_\gamma)] dE_\gamma.$$

By examining carefully a few cases of the entire distribution of the scintillation spectrum of a single  $\gamma$  ray at various energies we find that the Compton-electron distribution for a certain  $\gamma$  energy is approximately constant over the energy-range  $0 - E_\gamma^*$ . We can therefore approximate the function  $C(E, E_\gamma)$  to be

$$C(E, E_\gamma) = C(E_\gamma) = 1/E_\gamma^*, \quad 0 < E < E_\gamma^* \\ C(E, E_\gamma) = 0, \quad E > E_\gamma^*.$$

In order to obtain the Compton-electron distribution, we performed a step-by-step integration. One starts out at the highest energy and takes the  $N_a(E_\gamma)$  from curve (see Fig. 6). Then one looks up the corresponding  $[1 - p(E_\gamma)]$  and chooses a suitable value of  $\Delta E_\gamma$ , the smaller the better. One then calculates  $[\Delta N_c]_{E_\gamma}$ , the ordinate of the Compton distribution from 0 to  $E_\gamma^*$  due to photons of energy between  $E_\gamma$  and  $E_\gamma + \Delta E_\gamma$ , by the relation

$$[\Delta N_c]_{E_\gamma} = \frac{1}{E_\gamma^*} \cdot N_a(E_\gamma) [1 - p(E_\gamma)] \Delta E_\gamma.$$

This process is repeated throughout the spectrum and finally, by adding up all the contributions, we get the Compton-electron distribution (Curve C, Fig. 4). This must be added to the distribution curve due to photoelectrons (Fig. 4, Curve B).

#### D. Backscattering

Here it becomes important to investigate the influence of the surrounding material. The backscattering results partly from the glass window of the photomultiplier-tube and from the source and crystal containers and partly from the surrounding material, as Pb-shielding. It is important to remove as much surrounding material as possible and to try to measure the residual backscattered peak mostly due to the glass window and the source- and crystal-containers. This residual backscattered peak will always be present in all the measurements. The Pb shielding, that is necessary for the measuring of the weak inner bremsstrahlung, should be kept at a distance so as not to increase the backscattering. In this experiment it was

found that 2-in. Pb shielding at a distance of 6 in. from the source-crystal did increase the backscattering, but when the shielding was removed to a distance of 8 in. the increase in backscattering was negligible. Another effect that has to be taken into consideration is the fluorescence radiation from the Pb shielding. A thick aluminum lining of the Pb shielding is provided to take care of this effect. It is not advisable to put a Cu absorber close to the source- and crystal-containers to attenuate this radiation, since the backscattering thus produced is undesirable.

The correction for the backscattering is of course very difficult to calculate accurately. It is shown by an auxiliary experiment that at the energy of 661 keV and with proper geometry, the backscattered peak was about 9% of the photo peak. Considering the energy dependence of the Compton cross section, the  $\gamma$  efficiency and the original spectral intensity, it is estimated that the average number of backscattered photons is equal to 9% of the number of photoelectrons from photons of energy of 200 keV  $\rightarrow E_{\max}$ . The energy range for the backscattered photons is around 110 keV  $- 200$  keV with a tail to the high-energy side due to the 90°-scattered photons. [ $E_{90^\circ}$  for 800 keV = 310 keV]. This estimation leads to the curve D on Fig. 4.

#### E. K X-Ray Escape Effect

This correction has been calculated by Novey,<sup>13</sup> and since this is a surface effect the correction is not dependent on the thickness of the crystal. The correction is shown as curve E on Fig. 4.

#### F. Absorption

Of course the experimental arrangement should be arranged to reduce this effect to a minimum. In our case there is a limit since the source is in gas form. The total absorbing material between the source and the crystal is a 1-mil Al foil of the window of the gas container and a 1-mil Al foil on top of the crystal. The absorption effect does not show up until 30 keV and is shown as curve F in Fig. 4.

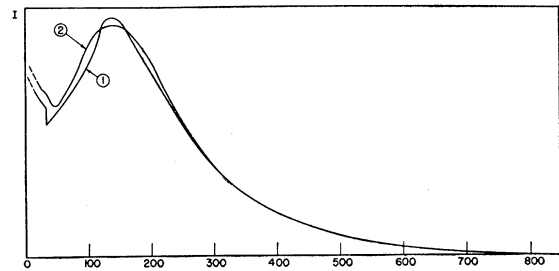


FIG. 7. The correction for the resolution of the system. Curve 1 is the total theoretical distribution,  $N_{\text{theor}}$ , obtained from Fig. 4. Curve 2 is the distribution,  $N_{\text{res}}$ , obtained by correcting  $N_{\text{theor}}$  for resolution as described in Sec. III(G).

<sup>13</sup> T. B. Novey, Phys. Rev. 89, 672 (1953).

### G. Effect of the Resolution of the System

The correct way to carry out this correction is to treat the theoretical distribution according to the known resolving power of the system and then to compare the resultant curve with the experimental one. If the continuous spectrum is considered to consist of a number of monochromatic  $\gamma$  rays it is obvious that each " $\gamma$  ray",  $E_\gamma$ , is recorded as a Gaussian distribution,  $g(E)$ ,

$$g(E) = [2\pi KE_\gamma]^{-\frac{1}{2}} \exp[-(E_\gamma - E)^2 / 2KE_\gamma],$$

where  $K = W^2(E_\gamma) / 2E_\gamma \ln 2$  and  $W(E_\gamma) =$  half-width at half-intensity.  $N_{\text{res}}$ , the theoretical distribution corrected for resolution, is therefore obtained by integrating:

$$N_{\text{res}}(E) = \int_0^{E_{\text{max}}} N_{\text{theor}}(E_\gamma) g(E) dE_\gamma.$$

This operation was carried out by graphical integration and the correction is shown in Fig. 7. At energies above 300 kev the corrected and the uncorrected curve coincide.

### H. Background

This correction is carried out on the experimental points and includes the tube-noise, the amplifier-noise and the background radiation. This correction is shown as "noise-level" in Fig. 8. The noise-level varies drastically with the room temperature, so all the measurements were taken in an air-conditioned room with a minimum temperature variation.

## IV. RESULTS

In Fig. 8 is shown the final theoretical curve together with the experimental points. The experiment was repeated in two runs with different gain on the amplifier.

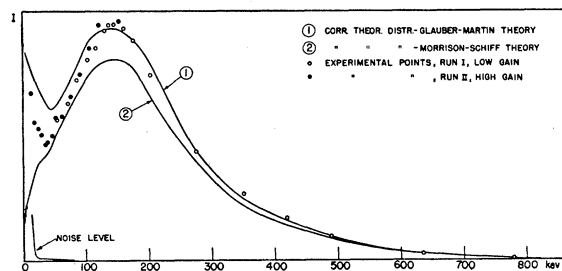
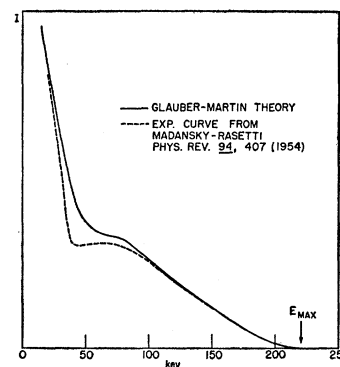


FIG. 8. Inner bremsstrahlung from A<sup>37</sup>. (1) Theoretical distribution according to the Glauber-Martin theory after correction for the experimental factors. (2) Theoretical distribution according to the Morrison-Schiff theory after correction for the experimental factors. ○—Experimental points, Run I, low gain. ●—Experimental points, Run II, high gain.

FIG. 9. A comparison of the experimental distribution of the inner bremsstrahlung from Fe<sup>55</sup> by Madansky and Rasetti (reference 3) to the theoretical prediction of Glauber and Martin.



The peak-counting rate at 150 kev in Run I is 3100 counts/min, and the experimental points are normalized to the theoretical curve by taking the average ratio of three points above 250 kev. The peak-counting rate in Run II is 750 counts/min and the exp points are matched to Run I at 90 kev.

The agreement down to 100 kev is excellent. Because of the low  $Z$ -value of A<sup>37</sup> ( $Z=18$ ), the contribution due to the  $2P$  electron capture does not become important until below 30 kev. The experimental distribution curve does reach a maximum around 150 kev as predicted and then drops down to 30 kev. From there it suddenly swings up rapidly. In fact, this occurs exactly where the effect of the  $2P$  electron-capture should show up as predicted by the Glauber and Martin calculation.

The experimental points below 120 kev do not lie exactly on the theoretical curve. This may be due partially to the accumulated errors introduced by the various corrections and partially to the simplifications used in the theoretical calculations. As Glauber and Martin pointed out, the screening effect on the distribution was not included in the calculation but it may be appreciable in the low-energy region. For comparison, we tried to fit the experimental distribution of the inner bremsstrahlung from Fe<sup>55</sup> by Madansky and Rasetti<sup>4</sup> to the theoretical prediction of Glauber and Martin (Fig. 9). We observed that the agreement was excellent to about 100 kev. Below that energy the experimental points were below the predicted values. The neglect of the screening effect would yield higher predicted values at the low-energy region.

We wish to thank Dr. P. C. Martin and Dr. F. Pollock for many enlightening and stimulating discussions, and Professor W. W. Havens, Jr., for his constant interest. One of the authors (T. L.) wishes to express his appreciation to the Department of Physics, Columbia University, for the opportunity of working in its laboratories and to acknowledge a grant from the Swedish Atomic Committee.